

# Interpretation of Triaxial Testing Data for Estimation of the Hoek-Brown Strength Parameter $m_i$

Bewick, R. P., Kaiser, P.K. and Valley, B.

*Centre of Excellence in Mining Innovation, Sudbury, ON, Canada*

Copyright 2011 ARMA, American Rock Mechanics Association

This paper was prepared for presentation at the 45<sup>th</sup> US Rock Mechanics / Geomechanics Symposium held in San Francisco, CA, June 26–29, 2011.

This paper was selected for presentation at the symposium by an ARMA Technical Program Committee based on a technical and critical review of the paper by a minimum of two technical reviewers. The material, as presented, does not necessarily reflect any position of ARMA, its officers, or members. Electronic reproduction, distribution, or storage of any part of this paper for commercial purposes without the written consent of ARMA is prohibited. Permission to reproduce in print is restricted to an abstract of not more than 300 words; illustrations may not be copied. The abstract must contain conspicuous acknowledgement of where and by whom the paper was presented.

**ABSTRACT:** Triaxial tests are conducted to determine the relationship between confinement and axial compressive strength. Depending on the confining stress applied to a core specimen, the failure process changes depending on the rock type's internal composition (i.e. porosity, flaws, stiffness heterogeneity, grain shape, etc.). These failure process changes are not typically considered when planning a triaxial testing program or when processing triaxial test data. This paper summarises the changes in failure process that occur depending on the confining stress level for various rock types and outlines a procedure for processing triaxial data depending on the confining stress level for the determination of the Hoek-Brown strength envelop parameter  $m_i$  and confidence intervals. For this, a triaxial and uniaxial dataset from Bingham Canyon is presented for a quartzite. The dataset is exceptionally complete in terms of the number of tests conducted (total of 217 uniaxial and triaxial tests) and the detail in test data quality and characterization of the specimens. The results show that triaxial data requires  $m_i$  values outside ( $m_i > 50$ ) the typically assumed range ( $m_i \leq 50$ ). These high  $m_i$  values appear to be needed to fit data at high confining stress levels (larger than about UCS/10). Based on the discussion in this paper; (1) the selection of confinement levels for testing purposes should include sufficient data in the confinement range of 0 to UCS/10 and UCS/10 to UCS/2; and (2) two sets of strength curves may need to be considered depending on the problem being assessed. One curve is valid for confinements of 0 to UCS/10 (representative of strengths near excavation boundaries) and the other for  $>UCS/10$  to approximately the Mogi line (representative of strengths, for example, in wide pillars or mine abutments), after which a third envelop is needed. These changing envelop requirements are a result of changing failure mechanisms.

## 1. INTRODUCTION

Recent developments in understanding brittle failure processes in hard brittle rocks ( $UCS > 25\text{MPa}$ ) has lead the authors to the realization that there are several deficiencies in how triaxial data is being treated to arrive at peak strength parameters. Furthermore, it is necessary to properly describe the uncertainty in test data. This paper aims at providing an understanding of how failure processes change as confinement increases, how this affects the failure envelop and thus how data should be interpreted to arrive at meaningful engineering parameters. Most importantly, as recently introduced by [1] it is necessary to differentiate strength envelops that are to be used for low confinement dominated problems (inner shell) and for those used to describe the behavior of rock at high confinement (outer shell).

The goals of this paper therefore are: (a) to review current practice for processing of triaxial data; (b) identify failure mechanisms that occur during loading at increasing confinement levels for different rock types and how they cause changes in the curvature of the strength envelop; and (c) provide suggested procedures

for the formulation of triaxial data testing programs and the processing of triaxial testing results.

### 1.1. Triaxial Testing in Mining and Civil Contexts

Triaxial testing programs on intact rock are typically conducted to determine: (a) the rock's general peak strength envelop over a practically relevant confining range; and (b) estimate parameters of empirical failure criteria such as the Hoek-Brown criterion considered here. In mining and civil related projects, triaxial tests are not typically undertaken or are with only a few specimen tested over a limited and often insufficient confinement range considering the failure mechanisms anticipated *in situ*. Furthermore, test data may show a wide range of scatter due to a mix of failure mechanisms from spalling to shear failure, with or without the influence of preexisting flaws in the rock.

These deficiencies lead to inadequate strength criteria that, when applied to design, may have serious practical consequences. If insufficient triaxial test data is available, the Hoek-Brown parameter  $m_i$ , for example, is either looked up from tables of published estimates, e.g. [2] or estimated from such relations as  $m_i \approx UCS/\sigma_t$ . The use of these methods will be shown to produce (often

excessively) conservative results for confining stress levels higher than approximately UCS/10. When very few triaxial tests are available, high strength outliers are commonly removed for no reason other than ensuring conservatism. When the Hoek-Brown parameter  $m_i$  is estimated using the method suggested by [3,4], without removing the high strength outliers, high  $m_i$ -values, outside the normally considered range  $m_i < 50$ , are obtained. When this occurs, the respective  $m_i$  values are typically discarded,  $m_i$  re-estimated with high strength outliers removed, or estimated from  $m_i \approx \text{UCS}/\sigma_c$ . When a large number of data points are available over a sufficient confinement range but with a wide scatter, the challenge is to find the best fit and confidence limits for the data.

These issues influence engineering decisions and may result in both conservative or non-conservative designs. It is therefore important to first understand why the triaxial strength envelop for hard brittle rocks (UCS > 25 MPa) is curved, i.e., how the failure modes change as confinement increases. Next, it is necessary to identify the confinement range relevant to the engineering problem and for what confinement range various approximations, such as  $m_i \approx \text{UCS}/\sigma_c$ , are applicable. Finally, a systematic approach needs to be used to obtain representative  $m_i$ -values and respective confidence limits.

## 2. FAILURE MECHANISMS IN TRIAXIAL COMPRESSION

The fact that the failure mechanism changes as the confinement range increases is typically not considered when a triaxial testing program is established. As a consequence, this change in failure process is ignored when processing triaxial test data. As is shown in this article, in hard brittle rock, these mechanisms control the shape of the strength envelop.

Depending on an intact rock type's internal structure (porosity, flaws, grain interlocking, stiffness heterogeneity, etc.), the confining pressure levels differ for the transitions from brittle fracture to semi-brittle fracture to ductile flow. The term brittle is used in this paper to indicate that tensile failure processes influence the strength. While this in general implies that the post-peak stress strain curve has a negative slope, the term brittle in the context of this paper is not meant to solely relate to the degree of post-peak weakening. While the transition conditions differ for different rock types, it is this change in failure process that leads to a distinctly curved failure envelop in hard rocks. Kaiser and Kim [5] highlight this in suggesting that there may actually be a change in curvature, and therefore an S-shaped failure envelop for hard brittle rocks.

The curvature and change in curvature in the strength envelop is only evident if sufficient test data is available in each mechanistic behavior zone (i.e., if triaxial test data is available to cover the range from 0 to about 0.3 (ideally to 0.5) UCS. Otherwise, the S-shape envelop described by [5] may not be observed.

Next, the mechanistic processes for the "yielding", non-elastic behavior, of crystalline rocks, porous rocks, and rocks constituted with some ductile minerals (e.g. marble) are summarized. The failure processes of Carrara marble will be highlighted due to the availability of data over specific confinement ranges and used to illustrate how changes in failure process cause changes in curvature in the strength envelop. Generalized transition zones, as evident from the data summarized in this paper and supported by previous assessments, e.g., [5] and [6], will be summarized.

### 2.1. "Yield" Mechanisms for Various Rock Types

For granite and other crystalline rocks, increased confining pressure leads to a change in micro-fracturing process [7, 8, 9] (Figures 1 and 2). At low confining pressure, the dominant process is by long tensile cracks (mode I) parallel to the main stress direction resulting in axial splitting type failure. As the confining pressure increases, growth of tensile cracks is inhibited and short en echelon arrays of tensile cracks form with the overall effect of producing, first, single tensile induced shear fractures across the specimen and then multiple (typically conjugate) tensile induced shear fractures. Shearing only occurs once sufficient tensile crack densities [10] are present or stresses are sufficient for the failure of rock bridges between micro-crack arrays.

For sandstones and other porous rocks (Figure 3), failure processes transition from tensile induced shear-enhanced dilatancy in the brittle field to tensile induced shear enhanced compaction in the semi-brittle to ductile field [11, 12, 13, 14]. As discussed by [12], dilatancy prior to peak stress is attributed to grain movements following inter-granular micro-cracking as grain contacts rupture at high shear and low normal stresses. This mechanism (and hence dilatancy) is inhibited at elevated confining pressures because grain contacts cannot be easily ruptured and grain-based failure starts to dominate. Near the peak strength, intra-granular cracking starts to operate. At low confining pressure this involves shear movement and grain rearrangements, resulting in overall shear-enhanced dilatancy. At high confining pressure, grain fracture leads to local porosity collapse (shear-enhanced compaction) expressed macroscopically as bulk cataclastic flow.



Fig. 1. Slabbing at 2600m depth in a quartzite [15] due to long axial tensile cracks propagating at low confinement near the excavation boundary. This is analogous to axial splitting of unconfined or lightly confined compression tests.



Fig. 2. Shear rupture consisting of an echelon array of tensile microcracks produced at higher confining stress levels [15]. This is analogous to shear planes formed in triaxial compression tests.

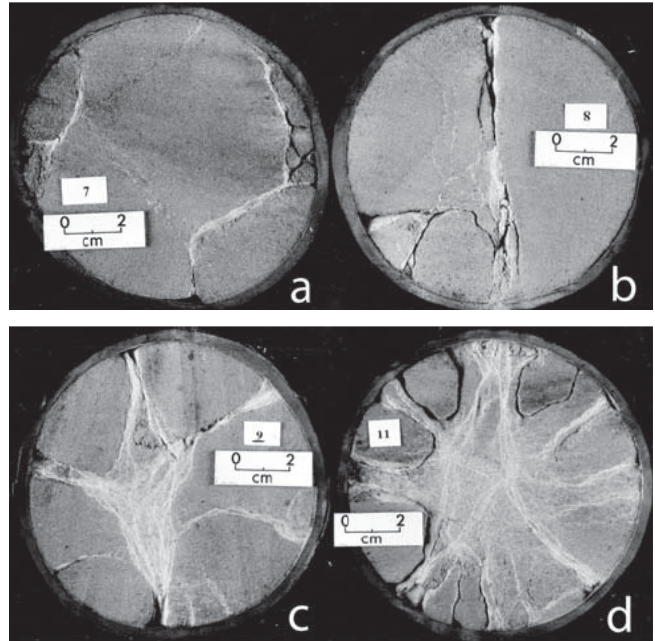


Fig. 3. Photos [12] showing radial cracking in cross sections perpendicular to  $\sigma_1$  of Locharbriggs sandstone deformed to 7.8% axial strain under confining pressures of: (a) 13.5MPa; (b) 27.3MPa; (c) 41.4MPa; and (d) 54.8MPa. Cores are cut. Core diameter: 100mm. Localization of deformation is expressed as pale distinct strands whose spatial characteristics change with increasing confining pressure.

For rocks containing abundant ductile minerals there is an interplay between cracking and crystal plasticity. As discussed by [16], crack propagation occurs when the tensile strength at the crack tips is reached. The increase of confining pressure tends to close the cracks and impedes their propagation. When dislocation glides or mineral plasticity occurs, the behavior is dominated by the applied shear stress and thus is relatively insensitive to confining pressure. Hence as the confining pressure increases, crack propagation is progressively replaced by plasticity as is the case for the Carrara marble discussed next.

The processes of hard brittle rock failure are not new and were observed by many, including [17]. Figure 4 summarizes observations of failure processes in a generalized brittle intact hard rock as represented by separate failure envelopes on the Mohr diagram. These zones are as follows (Figure 4):

1. Zone A (the elastic zone): un-fractured material, cataclastically unaffected; deforms either purely elastic or purely plastic; stress distribution at first is almost homogeneous; no structural material change occurs.
2. Zone B (crack initiation progressing towards damage): development of cataclastic cleavage fracturing (i.e., tensile cracks aligned with direction of loading). The test piece has become inhomogeneous. In the cataclastically affected

zones anisotropy arises. Principal deformation is permanent with lateral expansion.

3. Zone C (combined cataclasm) with intensive structural change: Combination of small cleavage fracturing, small shearing zones (a result of tensile cracking) and sliding movements (again only possible due to tensile crack arrays, no cracks propagate in mode II or III), which cause cataclastic plastic flow, resulting in collapse by shear in Zone D.
4. Zone D: collapse by secondary process of shearing along cataclastically granulated zone caused by tensile fracturing.
5. Zone E: zone of large cataclastic plastic flow at high triaxial loads, resulting in collapse by shear equal to Zone D.

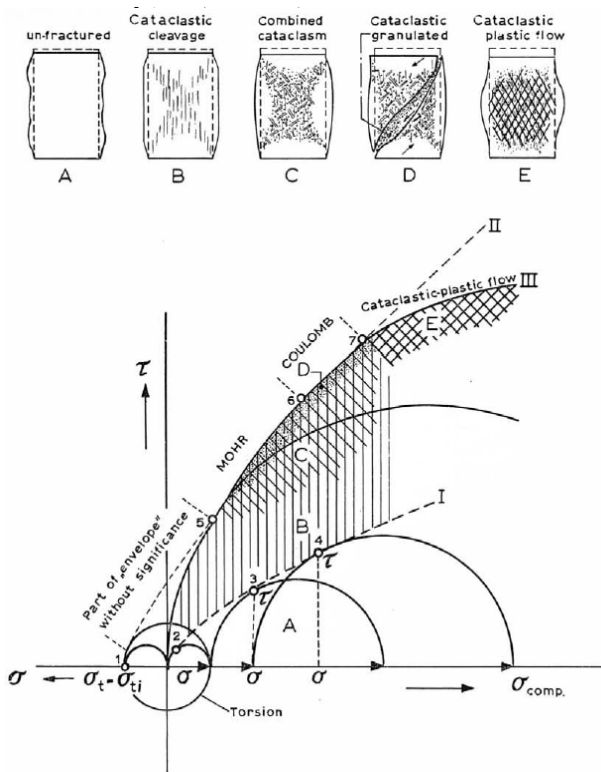


Fig. 4. Representation by Mohr-circles. Rock material passes through various structural stages when compressively loaded [17]. See text for description of annotations.

The transition in failure process is illustrated in the Mohr diagram in Figure 4:

- I – damage boundary between Zones A and B;
- II – envelop according to Mohr-Coulomb: branch for collapse by shearing after process of granulation;
- III – envelop according to Mohr-Coulomb; branch for large cataclastic plastic flow by internal combined cataclasm.

This figure illustrates that a transition between failure process leads to a non-linear failure envelop.

## 2.2. “Yield” Mechanisms and Strength Envelop Curvature for Marble

The triaxial testing data for Carrara marble for a range of confining pressures from 0 to 300 MPa using data from [18] and [19] is summarized in Figure 5. Figure 6 includes data from [18] alone to highlight the 0 to 35 MPa confinement range, various changes in curvature are evident. These are labeled in circles 1 through 5 and shown graphically with lines representing relatively consistent curvature trends. Based on the summary of yield modes using microscopic analysis techniques, [19] identified the various failure mechanisms that dominate depending on the confinement level. Observations of [19] coupled with the hypothesis of [5] which is summarized by [20] suggests that these inflection points occur due to changes in failure mechanisms. For labels 1 to 5 in Figures 5 and 6 these are as follows for Carrara Marble (based on [18] and [19]):

- (1) to (2) – Brittle Zone ( $0 \leq \sigma_3 \leq 30$  MPa): tensile cracks tend to grow across 3 to 4 grains and progressively shorten such that little tensile micro-cracking occurs around  $\sigma_3 = 30$  MPa. The influence of confining stress appears to change between  $\sigma_3 = 5$  MPa and 7.5 MPa or about UCS/10 (see Figure 6).
- (3) – Semi-Brittle Zone ( $30 \leq \sigma_3 \leq 85$  MPa): Yield is dominated at the grain boundaries but dislocation glide can occur once  $\sigma_3 > 50$  MPa.
- (4) – Semi-Brittle to Ductile Transition: near the Mogi Line (defined as  $\sigma_1/\sigma_3 = 3.4$ ) twinning begins to dominate initial yield. Twins start to be nucleation points for tensile crack propagation.
- (5) – Ductile:  $\sigma_3 \geq 300$  MPa yielding is dominated by crystal plasticity.

While [18] and [19] outline specific ranges, there are clear changes in envelop shape at approximately 10 MPa (confinement beginning to influence behavior) and 60 MPa (transition from brittle to semi-brittle) representative of the change in material behavior due to the changing failure processes occurring in the specimen.

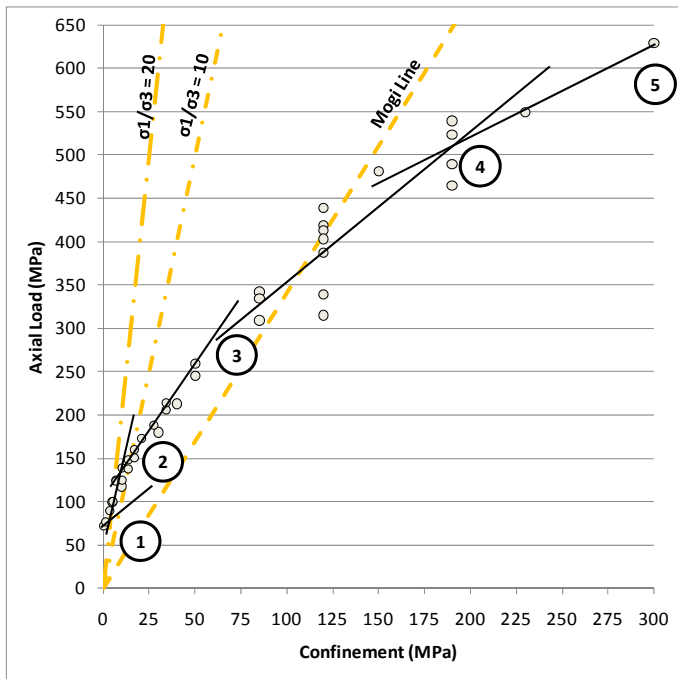


Fig. 5. Triaxial data on Carrara marble ([18] & [19]) showing changes in envelop curvature at various confinements as indicated by the inset numbers in circles and generalized trends in data represented by black solid lines. Lines 1 and 2 are more clearly defined in Fig. 6.

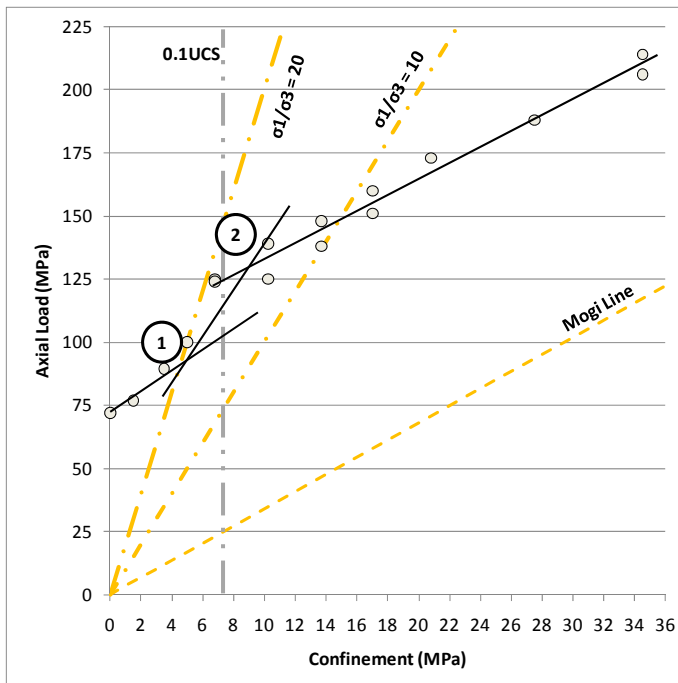


Fig. 6. Low confinement range of Fig. 5 showing triaxial data from [18]. A step change in the failure envelop is clearly evident at about UCS/10 or a stress ratio  $\sigma_1/\sigma_3$  of  $\sim 20$ .

### 2.3. Generalized Transition Zones

The above section describes the “yielding” mechanisms at different confinement levels for a marble which were linked to changes in curvature of the strength envelop. Different mechanisms dominate depending on the internal structure of a rock type. This is also shown for other rock types like Wombeyan marble, Figure 7 [21]

and Potash loaded at a rate of 1.75 microstrain per second, Figure 8 [22]. The insets in Figures 7 and 8 show the deformation and fracture styles which depend on confinement and change the shape of the strength envelop (see figure caption for details).

Not every hard brittle rock type tested in triaxial compression should be anticipated to display significant changes in envelop slope or curvature, but, two broad transition zones can generally be observed to influence the strength envelop shape and thus should be taken into account when determining the confinement ranges to be used when testing and processing triaxial test data. These are: (1) UCS/10 – the transition from failure processes involving tensile crack propagation to failure with tensile crack induced shear banding; and (2) Mogi line – the transition, in most cases, to ductile behavior (with no to little post-peak strength loss).

Next, a dataset will be used to fit the Hoek-Brown empirical strength envelop to show that different fits are required for different confinement ranges if the strength envelop is to be properly determined and that the use of the two transition zones discussed above can be used to aid in the processing of triaxial data.

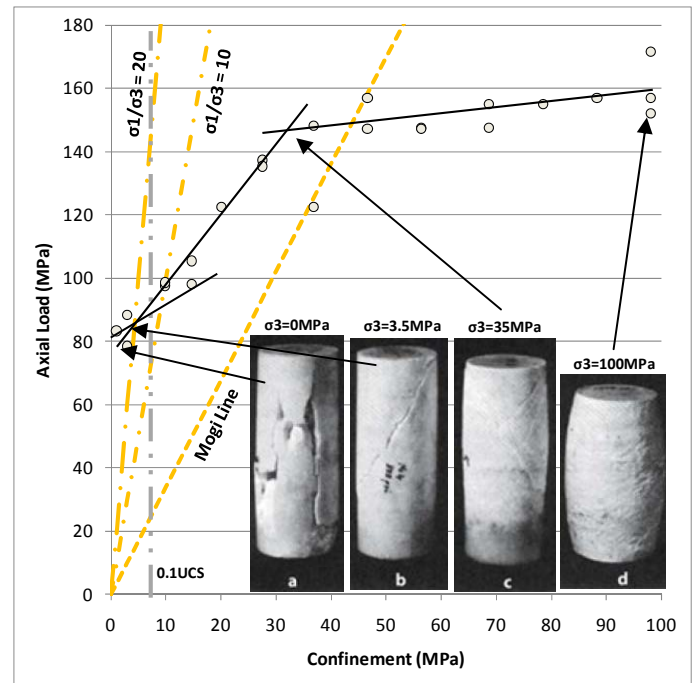


Fig. 7. Triaxial testing data on Wombeyan marble from [21] showing step-changes in envelop slope or curvature. Inset core specimen show change in failure mechanism with increasing confining stress level.

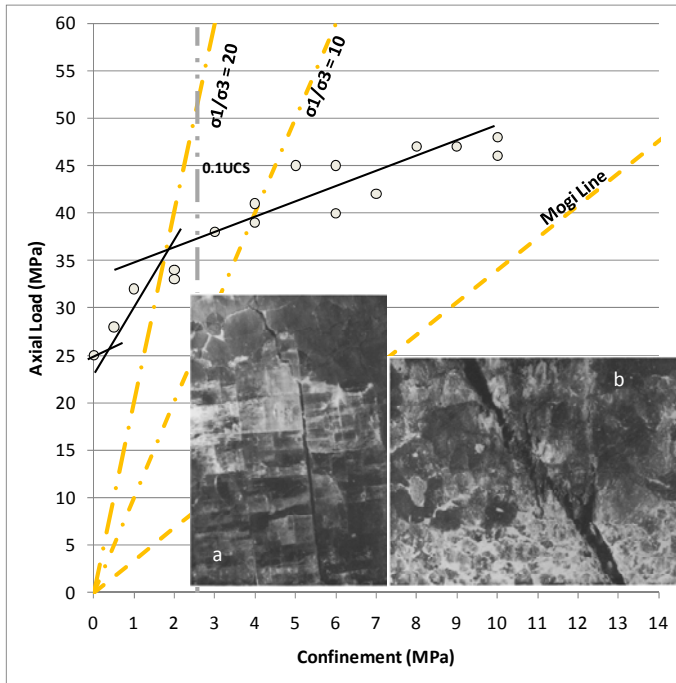


Fig. 8. Triaxial testing data on potash from [22]. Tests were completed at a constant strain rate of 1.75 microstrain per second. Changes in envelop curvature are evident and appear to related to failure mechanisms changes. Inset (a) shows low confining stress axial tensile microcracking; (b) shows higher confining stress en echelon array of microcracking. Confinement inhibits microcracking such that en echelon arrays are produced.

### 3. PROCESSING TRIAXIAL DATA

In this section, a triaxial and uniaxial dataset from Bingham Canyon is presented for a quartzite (Figure 9). The dataset is exceptionally complete in terms of the number of tests conducted (217) and the detail in test data quality and specimen characterization. The dataset has been fit to estimate the UCS and  $m_i$ -value using different methods and portions of the data as shown in Figure 9 which included the following (reference numbered curves in Figure 9):

1. Published  $m_i$ -values from [2];
2. The empirical relationship,  $m_i \approx \text{UCS}/\sigma_t$  (using the average UCS value);
3. Fitting procedure of [4] using the data with confinement levels  $\leq 10\text{MPa}$  ( $\approx \leq \text{UCS}/10$ );
4. Fitting procedure of [4] for all the data; and
5. Fitting procedure of [4] using the data with confinement levels  $> 10\text{MPa}$  ( $\approx > \text{UCS}/10$ ).

The above listed will be discussed in more detail in the following text.

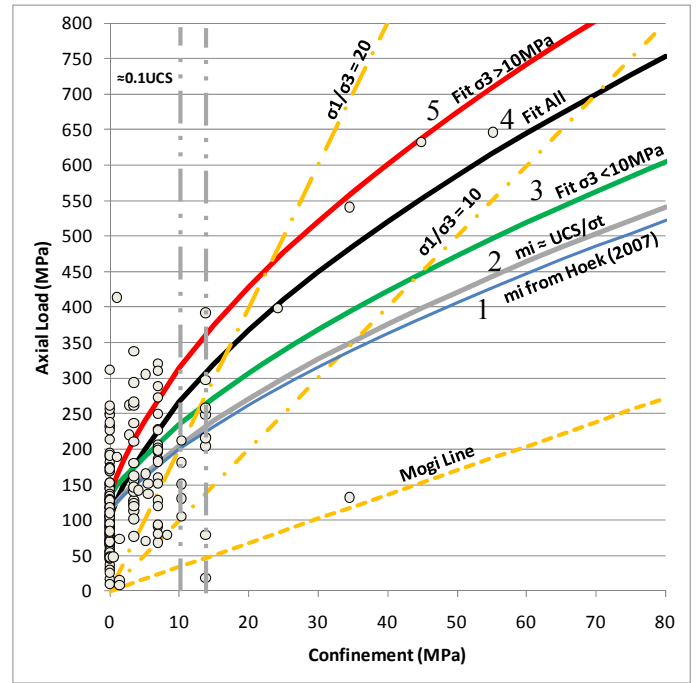


Fig. 9. Triaxial test data from a quartzite: the failure mechanisms in this dataset only include failure by intact rock breakage (by spalling and shear). Various Hoek-Brown envelopes are shown and explained in the text.

For the estimation of the UCS and  $m_i$  values for the quartzite, let us assume that we are progressing a mining project from scoping level ( $\pm 50\%$  of the financials) to pre-feasibility ( $\pm 25\%$  of the financials) and finally to feasibility ( $\pm 15\%$  of the financials). At the start, at scoping level, typically only uniaxial compressive strength and Brazilian testing data are available. The average UCS for the quartzite based on a confinement level of 0 MPa is 114 MPa with an excessively large standard deviation of 59MPa. The Brazilian strength is approximately 7.4MPa $\pm 4$  (again with a very large standard deviation). The Brazilian data is not shown. Assuming that the direct tensile strength of a rock is approximately 70% of the Brazilian strength, the estimated average tensile strength is 5.2 MPa. Based on this data and considering only the mean values (at scoping level), the estimated  $m_i \approx \text{UCS}/\sigma_t \approx 22$  which compares well with published values from [2] giving a range of  $20 \pm 3$  for a quartzite. Based on this, one would feel confident that the two lowest strength envelopes (numbers 1 and 2), Figure 9 (shown in light blue and grey respectively), are reasonable average strength estimates (the other curves on this figure will be explained below).

Next, let's assume that some triaxial testing has been completed and data up to a confinement level of 10 MPa (about UCS/10) is available, e.g., for the pre-feasibility study. Using the procedure proposed by [3,4] one would estimate an  $m_i = 23$  with a UCS of 138 MPa. Again,  $m_i$  would be deemed reasonable compared to the  $\text{UCS}/\sigma_t$  approximation used in the scoping study and to values

and range proposed by [2]. The updated envelop is plotted on Figure 9 in green (number 3, third from bottom).

Next, based on the recommendations of [3,4], data should be available to UCS/2 for strength envelop fitting, let's add the high confinement test data for UCS/10 to UCS/2 (about 50 to 70 MPa confinement), e.g., for the feasibility study stage. Again, using the procedure proposed by [3,4],  $m_i$  is now estimated as 54 with a UCS of 102MPa. This  $m_i$  estimate for the full confinement range is almost double the typically assumed  $m_i$  range of values for a quartzite. This final envelop is plotted on Figure 9 in black (second from top, curve number 4). It should be noted that the software package RocLab (©RocScience) does not allow one to obtain values  $> 50$  for  $m_i$ .

Comparing the curves and summary of UCS and  $m_i$  values (Table 1), based on the data, it is obvious that the envelops based on  $m_i \approx \text{UCS}/\sigma_1$  (curve 2 Figure 9), the  $m_i$  value proposed by [2] (curve 1 Figure 9), and the data based on triaxial testing up to 10 MPa (curve 3 Figure 9) greatly underestimate the strength of the rock at confinement levels greater than 10 MPa but appear reasonable for confinement levels less than 10 MPa. The fit through all the data (second envelop from the top, curve 4) under predicts the strength above a confinement level of about 25 MPa.

To arrive at a best fit for the high confinement range (UCS/10 to UCS/2), data with confining stresses  $>10$  MPa were used with the UCS estimated from the fit of the data from the confining stresses  $\leq 10$  MPa (this was required as the method proposed by [3,4] did not produce a UCS value). The resulting  $m_i$  value = 65 with a UCS of 135 MPa (red, uppermost curve, #5, in Figure 9). This fit seems to overestimate the strength in the confinement range  $\leq 10$  MPa. The implications of this will be discussed below but it is evident that standard triaxial data fitting procedures for this dataset do not produce a strength envelop that fits the entire dataset well. However, if the data is treated separately on either side of about UCS/10 (curve 5 and curve 3), the data appears well represented but a discontinuity would be encountered at UCS/10.

Table 1. Summary of envelop fits for the quartzite.

Fit	UCS (MPa)	$m_i$
Fit to All Data	102	54
Low Confinement Range Fit ( $\sigma_3 \leq 10$ MPa)	135	24
High Confinement Range Fit ( $\sigma_3 > 10$ MPa)	114	65
$m_i \approx \text{UCS}/\sigma_1$	114	22
Hoek (2007) [2]	/	20±3

To summarize, in hard brittle rock there is an S-shaped failure envelop. The failure envelop cannot be properly assessed unless sufficient data is available in the low ( $\sigma_3 \leq \text{UCS}/10$ ), moderate ( $\text{UCS}/10 < \sigma_3 < \text{UCS}/20$ ), and high ( $\sigma_3$  up to  $\text{UCS}/2$ ) confinement intervals. Due to the pre-dominance of tensile failure processes for hard brittle rock up to approximately UCS/10 [20] it is necessary to assess confidence intervals in triaxial data separately (i.e. for  $\sigma_3 \leq \text{UCS}/10$  and  $\sigma_3 > \text{UCS}/10$  up to  $\text{UCS}/2$ ).

#### 4. DETERMINATION OF CONFIDENCE INTERVALS

Due to a change in failure process in the quartzite at about UCS/10, it is necessary to estimate confidence intervals for strength envelops considering two different confinement ranges ( $\leq$  and  $> \text{UCS}/10$ ). The following procedure has been used to estimate potential strength envelops for the  $\pm 25\%$  confidence intervals and  $\pm 1$  standard deviation as shown on Figures 11 to 13 for all the data, data for confinement levels  $\leq 10$ MPa, and for confinements levels  $> 10$ MPa:

1. Estimate  $m_i$  and UCS based on [3,4].
2. Estimate the  $\pm 25\%$  confidence intervals:
  - a. Calculate the degree of freedom (the number of data points less the number of parameters in the function). The number of parameters in the function is 2 (i.e.  $m_i$  and UCS). For the entire dataset the degree of freedom is  $217 - 2 = 215$ .
  - b. Calculate the standard error for the measured yield strength relative to the fit strength envelop. Standard error uses the degree of freedom as an input parameter.
  - c. Calculate the critical t-value at the significance level of interest (i.e. 25% confidence interval would be calculated for 0.75). The critical t-value is a function of the degree of freedom as well.
  - d. Calculate the confidence interval magnitude which is the critical t-value multiplied by standard error.
  - e. Add or subtract the confidence interval magnitude from the fit to obtain the upper and lower confidence bounds.

One or multiple standard deviation or other confidence intervals can be calculated in a similar way by simply changing the critical t-value parameter (i.e. change to 0.05 for 95% confidence intervals).

3. Since confidence intervals are produced from  $\sigma_1$  and  $\sigma_3$  values, each confidence interval or deviation interval can be fit to estimate the  $m_i$  and UCS values using [3,4].

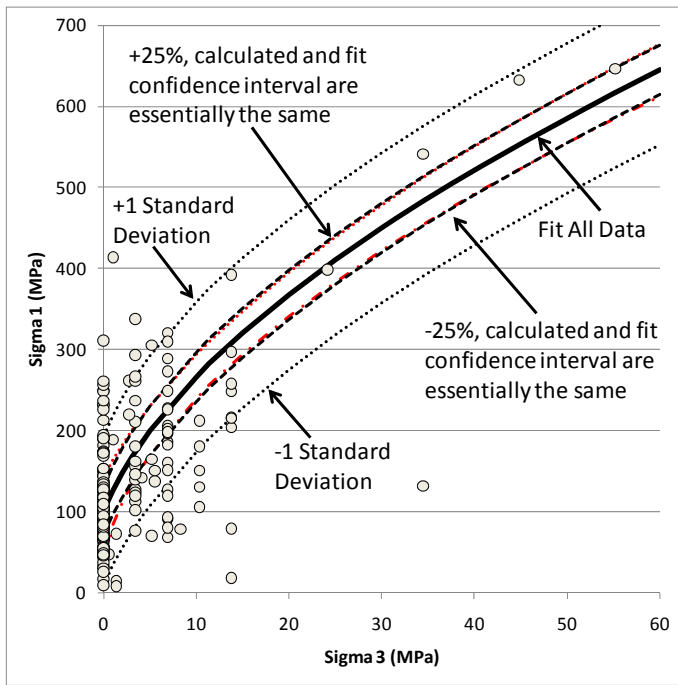


Fig. 11.  $\pm 25\%$  confidence intervals and  $\pm 1$  standard deviation for all data from the quartzite. The fit to the 25% confidence intervals have  $R^2$  of 1.0 so the fit directly overlaps the confidence interval.

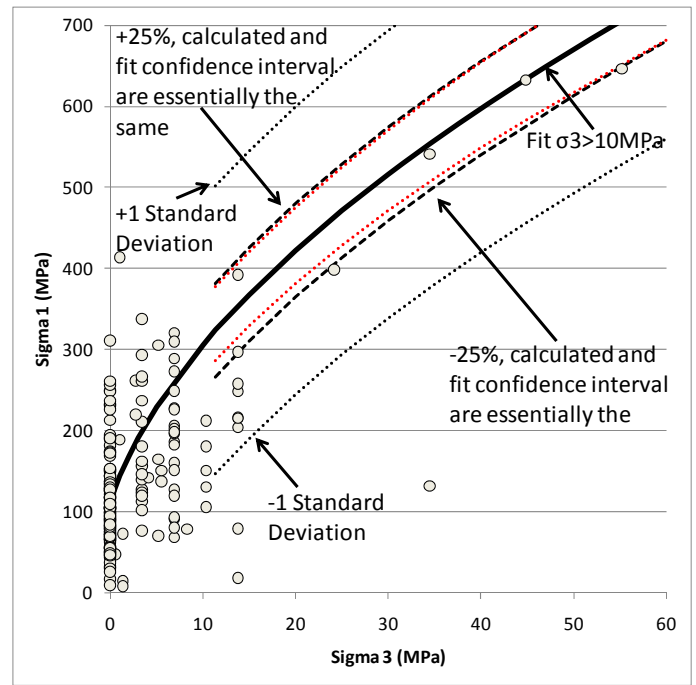


Fig. 13.  $\pm 25\%$  confidence intervals and  $\pm 1$  standard deviation for quartzite data  $\sigma_3 > 10$ MPa. The fit to the 25% confidence intervals have  $R^2$  of 1.0 so the fit overlaps the confidence interval.

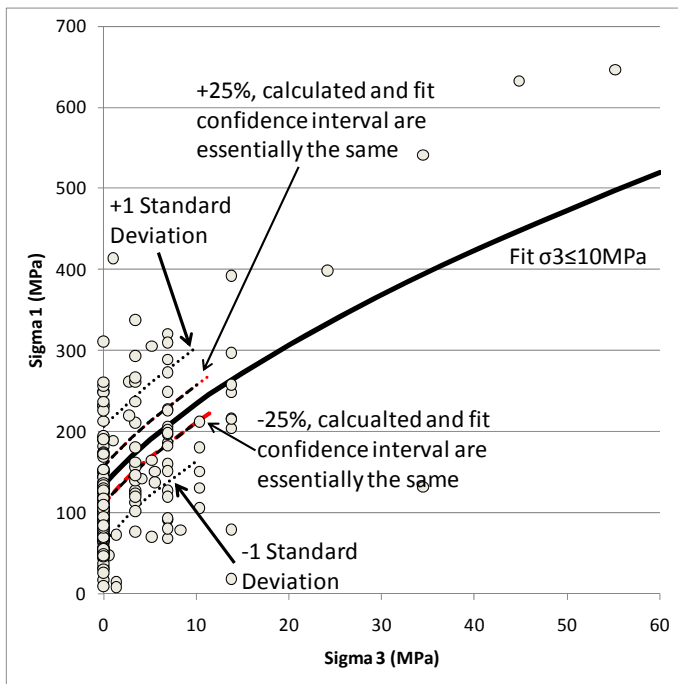


Fig. 12.  $\pm 25\%$  confidence intervals and  $\pm 1$  standard deviation for quartzite data  $\sigma_3 \leq 10$ MPa.

Note that in some cases the procedure of [3,4] does not produce a fit. This was the case when attempting to fit the -25% interval of the confinement data  $> 10$  MPa. The resulting envelop presented in Figure 13 is an estimation of visual fit by trial and error. Table 3 summarizes the  $m_i$ , UCS and  $R^2$ -values for the fits to the confidence intervals and Figure 14 summarizes the corresponding low and high end confidence envelopes.

Table 3. Summary of envelopes for  $\pm 25\%$  confidence interval fits for the quartzite.

Fit	UCS (MPa)	$m_i$	$R^2$
+25% All Data	144	42	1.00
Mean All Data	102	54	
-25% All Data	45	113	1.00
+25% $\sigma_3 \leq 10$ MPa	159	23	1.00
Mean $\sigma_3 \leq 10$ MPa	135	24	
-25% $\sigma_3 \leq 10$ MPa	111	25	1.00
+25% $\sigma_3 > 10$ MPa	192	44	1.00
Mean $\sigma_3 > 10$ MPa	114	65	
-25% $\sigma_3 > 10$ MPa	56	114	1.00

The most striking observation from Table 3 is that the  $m_i$ -values with the exception of those for three fits (for confinement  $\leq$  UCS/10) are much higher than those obtained from standard fitting techniques, including the use of RocLab (©RocScience). The  $m_i$ -values  $> 50$  as obtained for 4 envelopes are far beyond those considered acceptable using standard procedures. However, as the fits in the respective figures show, they correctly reflect the data.

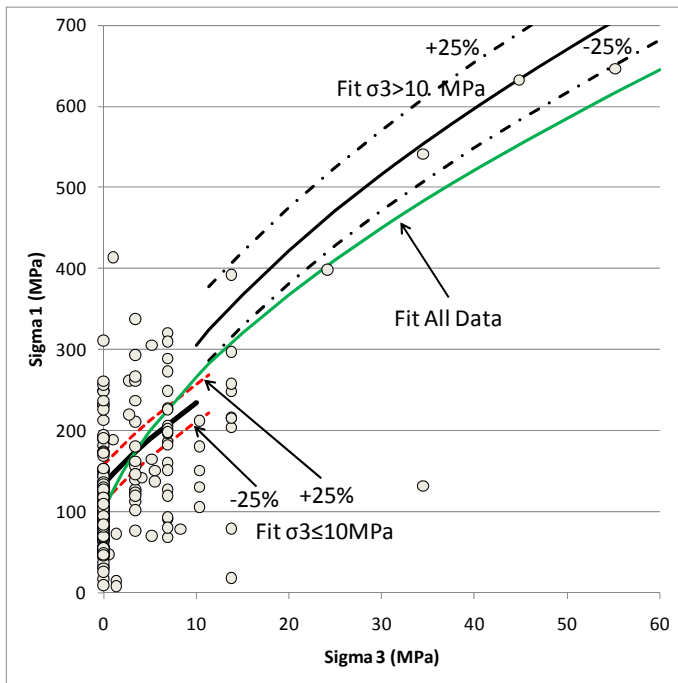


Fig. 14.  $\pm 25\%$  confidence intervals for quartzite data  $\sigma_3 \leq 10\text{MPa}$  and  $\sigma_3 > 10\text{MPa}$ . Also shown is the fit for the entire dataset.

## 5. DISCUSSION

### 5.1. Estimation of $m_i$ for low and high confinement ranges

Triaxial testing data was assessed using different methods and subsets of the data producing significantly different  $m_i$ -values. Clearly, the use of the suggested  $m_i$  values from [2] yield, in some cases, extremely conservative estimates of strength for confining stress levels greater than about  $UCS/10$ .

Estimating the  $m_i$  value for confinement levels greater than  $UCS/10$  resulted in  $m_i$ -estimates outside the typical range of values (i.e.,  $m_i$  values were generally  $>50$ ).

The data interpretation presented in this paper suggests that to arrive at representative strength estimates, parameters should be obtained separately for low confining stress levels up to  $UCS/10$  and for high confinement ranges  $>UCS/10$ .

The implications of the changes in strength envelop parameters are particularly relevant for pillars with intermediate to large width to height ratios, where the pillar core remains confined. For such cases, the strength of the pillar core is potentially much higher than would be estimated by a single fit relationship. An evaluation of the impact of this hypothesis on pillar strength is developed in [1] by considering an S-shaped criterion which can be thought of as being a linkage of two separately fitted envelopes for the low and high confinement ranges as discussed in this paper. For small W/H ratios, failure is dominated by spalling and both

single and multiple (low and high confinement) fits lead to representative envelopes.

The consequences for pillar design are two-folded: 1) pillar design can possibly be optimized, using smaller W/H ratios still insuring the carrying capacity of the pillar, and 2) pillars that would be assumed to be yielding (relaxed) with a failure envelop based on a single fit could have a core in pre-peak conditions, i.e. accumulating stress and potentially entering into a more burst prone behavior state.

### 5.2. Confidence Intervals

Confidence intervals can be estimated from triaxial datasets and those intervals fit to estimate the UCS and  $m_i$ -values resulting in lower and upper bound strength envelopes. These envelopes can then be used in numerical stress modeling to constrain potential stable and yielding conditions.

In order to fit some of the confidence intervals, higher than normal  $m_i$  values were obtained (i.e.  $>50$ ).

It should be noted that the confidence intervals on lab samples cannot be directly transferred to the rock mass strength. Scale effects have a major effect on the confidence limits of the rock mass strength.

## 6. CONCLUSIONS

The triaxial data in this paper suggests that:

- When planning a triaxial data testing program, confinement levels from  $\leq UCS/10$  and  $>UCS/10$  should be obtained; ideally up  $UCS/2$ . If such confinements cannot be reached for very strong hard brittle rocks, the data interpretation must consider the potential lack of information in the high confinement zone.
- Using published  $m_i$  values from [2] is reasonable for confinements  $\leq UCS/10$ , that is near excavations. For higher confinements, the published values appear to be extremely conservative.
- Using the  $m_i \approx UCS/\sigma_1$  relationship is reasonable for confinements  $\leq UCS/10$  and, similar to above, leads to very conservative strengths at higher confinement levels.
- Although not shown in this paper, uncertainty in tensile strength when using the fitting procedure of [3,4] can significantly influence the estimated strength parameters and strength envelop shape. The currently accepted fitting procedure needs refinement.
- $m_i$  values greater than 50 are needed in some cases to fit triaxial data for brittle rocks over the entire confinement range to  $>UCS/10$ . Based on the data analyzed here, such high  $m_i$ -values seem representative and thus practical for brittle rocks.

- Separate fits for 0 to UCS/10 and > UCS/10 range should be considered when processing triaxial data, especially when dealing with deep or high stress mining environment where different failure mechanisms may be occurring due to confining stress levels; e.g., in wide pillars.
- A procedure for the estimation of confidence intervals was presented. It was shown that the fitting procedure of [3,4] can be used to estimate the UCS and  $m_i$  values that apply to the confidence intervals.

## ACKNOWLEDGMENTS

The authors would like to thank staff at Kennecott Utah Copper (KUCC), Bingham Canyon Mine, and Rio Tinto for providing the data and for permission to publish it. Support from the Natural Sciences and Engineering Research Council of Canada (NSERC) is gratefully acknowledged.

## REFERENCES

1. Kaiser, P. K., B.H. Kim, R.P. Bewick, B. Valley. 2010. Rock mass strength at depth and implications for pillar design. In: Van Sint Jan, M., Potvin, Y. (Eds.), *Deep Mining 2010 - 5th international seminar on deep and high stress mining*, Santiago, Chile. Australian Center for Geomechanics, pp. 463-476.
2. Hoek, E. 2007. *Practical Rock Engineering*.
3. Hoek, E. and E.T. Brown. 1980. *Underground Excavations in Rock*. London: Inst. Min. Metall. 527 pages.
4. Hoek, E. and E.T. Brown. 1997. Practical estimates of rock mass strength. *Int. J. Rock Mech. Min. Sci.* 34: 8,1165–1186.
5. Kaiser, P. K. and B.H. Kim. 2008. Rock mechanics advances for underground construction in civil engineering and mining. In: Korean Symposium of Rock Mechanics.
6. Mogi, K. 1966. Pressure Dependence of Rock Strength and Transition from Brittle Fracture to Ductile Flow. *Bulletin of the Earthquake Research Institute*. 44, 215-232.
7. Velde, B., D. Moore, A. Badri, and B. Ledesert. 1993. Fractal analysis of fractures during brittle to ductile changes. *J. Geophys. Res.* 98(B7), 11,935-940.
8. Jaeger, J.C. and N.G.W. Cook. 1979. *Fundamentals of Rock Mechanics*. Chapman and Hall, New York.
9. Escartin, J., G. Hirth, and B. Evans. 1997. Nondilatant brittle deformation of serpentinites: Implications for Mohr-Coulomb theory and the strength of faults. *J. Geophys. Res.* 102(B2), 2897-2913.
10. Lockner, D.A., Moore, D.E. and Reches, Z. 1992. Microcrack interaction leading to fracture. *Rock Mechanics*, (eds. Tillerson and Wawersik), Rotterdam: Balkema, 807-816.
11. Mair, K., I. Main, and S. Elphick. 2000. Sequential growth of deformation bands in the laboratory. *J. Struct. Geol.* 22, 25-42.
12. Mair, K., S. Elphick, and Main, I. 2002. Influence of confining pressure on the mechanical and structural evolution of laboratory deformation bands. *Geophys. Res. Letters*. 29(10), 1410, 10.1029/2001GLO13964.
13. Wong, T.F., C. David, and W. Zhu. 1997. The transition from brittle faulting to cataclastic flow in porous sandstones: Mechanical deformation. *J. Geophys. Res.* 102, 2009-3025.
14. Menendez, B., W. Zhu, and T.F. Wong. Micromechanics of brittle faulting and cataclastic flow in Berea sandstone. *J. Struct. Geol.* 18, 1-16.
15. Ortlepp, D. 1997. Rock Fracture and Rockbursts. The South African Institute of Mining and Metallurgy.
16. Amitrano, D. 2003. Brittle-ductile transition and associated seismicity: Experimental and numerical studies and relationship with the b value. *J. Geophys. Res.* 108(B1), 2044, doi:10.1029/2001JB000680.
17. Gramberg, J. 1965. Axial Cleavage Fracturing, A Significant Process in Mining and Geology. *Engineering Geology*, 1(1), 31-72.
18. Gerogiannopoulos, N.G. 1976. A Critical State Approach to Rock Mechanics. Ph.D. thesis, University of London.
19. Fredrich, J.T. and B. Evans. 1989. Micromechanics of Brittle to Plastic Transition in Carrara Marble. *J. Geophys. Res.* 94(B4), 4129-4145.
20. Valley, B., Suorineni, F. T. and Kaiser, P. K., 2010. Numerical analyses of the effect of heterogeneities on rock failure process. In 44th U.S. Rock Mechanics Symposium and 5th U.S.-Canada Symposium, pages 10-648.
21. Patterson, M.S. 1958. Experimental deformation and faulting in wombeyan marble. *Geological Society of America Bulletin*. 69, 465-476.
22. Carter, B.J., E.J. Scott Duncan, and E.Z. Lajtai. (1991). Fitting strength criteria to intact rock. *Geotechnical and Geological Engineering*. 9, 73-81.